Chapter 2
Tropical Cyclone Multiscale Wind Features from Spaceborne Synthetic Aperture Radar

Jun A. Zhang and Xiaofeng Li

Abstract This study presents multi-scale wind features observed in space-borne synthetic aperture radar (SAR) images in tropical cyclones. Examples of eyewall mesovotices, spiral rainbands, fine-scale-band features, arc clouds, and boundary layer rolls are documented. Although these wind features are strongly tied to tropical cyclone dynamics and intensity based on previous numerical studies, they are not well-observed due to high rainfall and cloudiness that limits remote sensing instrument and severe environment for in-situ observations to survive. Since SAR images view the actual ocean surface responses to the storm-forced winds, they provide clear evidence for the presence of these wind features below clouds and their interaction with the sea surface. Analyses of the characteristics of boundary layer rolls based on SAR images show good agreement with in-situ aircraft observations, suggesting that a SAR image has a great potential to be utilized to study tropical cyclone low-level structure.

2.1 Introduction

Hurricanes account for a significant portion of damage, injury and loss of life from natural hazards, and are the most expensive natural catastrophes in the US [1]. The threat of high winds and storm surge has been known for intense storms. Multiscale wind features such as the "eyewall mesovortices", spiral band features, and boundary layer wind streaks or rolls are believed to largely contribute to the hurricane induced damage during landfalls. These features are also strongly tied to hurricane dynamics according to previous observational and numerical modeling studies.

J.A. Zhang (✉)
National Oceanic and Atmospheric Administration (NOAA)/AOML/Hurricane Research Division, University of Miami/CIMAS, Miami, FL, USA
e-mail: jun.zhang@noaa.gov

X. Li
GST, National Oceanic and Atmospheric Administration (NOAA)/NESDIS, College Park, MD, USA
e-mail: xiaofeng.li@noaa.gov

X. Li (ed.), *Hurricane Monitoring With Spaceborne Synthetic Aperture Radar*, Springer Natural Hazards, DOI 10.1007/978-981-10-2893-9_2

Previous observations have shown that intense transient vorticity features usually exist close to the inside edge of eyewalls of numerous intense hurricanes. Marks and Houze [2] reported the first example of eyewall mesovortices in Hurricane Debby (1982) using airborne Doppler radar data. Mesovortices were also seen in satellite images in Hurricane Isabel (2003) by Kossin and Schubert [3] and analyzed in Doppler radar data in Hurricane Guillermo (1997) by Reasor et al. [4]. Such vortical features are also clearly shown in several recent high-resolution cloud-representing numerical model simulations [5, 6], as well as in two-dimensional turbulence-resolving numerical models [7, 8]. The mesovortices are tied to the combined baratropic-baroclinic instability that is associated with the annulus of high potential vorticity near and within the eyewall clouds. Eyewall mesovortices have horizontal scales smaller than the diameter of the hurricane eye, but generally larger than the scales of individual cumulus clouds that constitute the eyewall.

Well-organized bands of convection and precipitation are commonly observed in and around a hurricane in satellite and radar images, which are usually called "spiral bands". Through careful analysis of land-based Doppler radar data of landfalling hurricanes, Gall et al. [9] identified a new class of spiral bands which are called "fine-scale spiral bands", and are significantly smaller than the rainbands (with $\sim$100 km scale) typically visible in satellite images. The radial wavelengths of the fine-scale spiral bands are between 5–10 km. Numerical simulations of landfalling hurricanes also identified features with similar wavelengths extending through the depth of the troposphere [10–12]. Katsaros et al. [13] identified roll-like structures with similar horizontal wavelengths (4–6 km) in the convection-free areas between the larger rainbands of several hurricanes through analysis of synthetic aperture radar (SAR) images. Nolan [14] investigated the mechanisms for the fine-scale spiral bands in the hurricane boundary layer using idealized numerical simulations and showed that an instability associated with the inflection points of the swirling boundary layers is a good candidate mechanism.

Boundary layer secondary-circulations or 'roll vortices' are known to be a common feature in the atmospheric boundary layer which have a significant influence on turbulent exchange of momentum, sensible heat and latent heat. Satellite remote sensing and Doppler radar observation indicate that rolls frequently form in the hurricane boundary layer. Wurman and Winslow [15] provided the first evidence of intense subkilometer-scale horizontal roll vortices in the high resolution Doppler radar wind retrievals in the boundary layer of Hurricane Fran (1996) during landfall. Morrison et al. [16] analyzed a large quantity of Weather Surveillance Radar-1998 Doppler (WSR-88D) data during landfalls of three hurricanes. They found rolls in 35–69% radar volumes which have a typical wavelength of 1450 m. They also found that the rolls were nearly aligned with the mean boundary layer wind. Lorsolo et al. [17] analyzed the data from the Shared Mobile Atmospheric Research and Teaching (SMART) radars in Hurricane Frances (2004) and found that the majority of wavelengths of rolls that are omnipresent in their data are between 200 and 650 in agreement with the study of Wurman and Winslow [15]. Ellis and Businger [18] analyzed WSR-88D data in two Typhoons and investigated a total of 99 cases of coherent structures and confirmed prior findings of roll observations. Foster [19] has developed a theory for roll vortices in curved flow at high wind speeds, such as in hurricanes, suggesting that hurricane boundary layer rolls transport high-momentum air from the upper boundary layer downward and enhance the transport of air-sea flux.

Since the first spaceborne microwave SAR onboard the National Aeronautics and Space Administration (NASA) SEASAT was launched in 1978 [20], tropical cyclones have also been observed by SAR images. Prior to the 2002 hurricane season, the "Hurricane Watch" program was established by the Canadian Space Agency (CSA) and Canadian Centre for Remote Sensing (CCRS) in collaboration with the National Oceanic and Atmospheric Administration (NOAA) Hurricane Research Division (HRD) flight planning team and the NOAA Aircraft Operations Center (AOC). This program helped collecting a large number of RADARSAT SAR images in and around hurricanes. SAR images were also collected in hurricanes when collocated in-situ aircraft observations were available [21]. A SAR image shows the sea surface imprint of a tropical cyclone, allowing us to extract multiscale wind features mentioned above.

2.2 Eyewall Mesovortices

It is often observed in mature hurricanes the low-level stratus or stratocumulus cloud decks in their eyes with vortical or "swirling" features embedded in these clouds. The swirling patterns in these eye clouds have different shapes ranging from circles centered in the eyewall to convoluted patterns with multiple swirls at various locations in the eye [22]. These swirling features usually observed at the inner edge of the eyewall are called "eyewall mesovortices" and are believed to form through Kelvin–Helmholtz instability [23]. Because of the concentrated angular momentum of the parent vortex into a small area, eyewall mesovortices can produce swaths of enhanced destruction for landfalling hurricanes [24]. They can also threat the operational safety of reconnaissance aircraft penetrating the hurricane eyewall [25]. Montgomery et al. [26] presented observational evidence that high-entropy air inside the low-level eye can sustain the storm at intensity above that predicted by the maximum potential intensity theory of Emanuel [27]. They suggested that the eye-eyewall mesovortices may be responsible for transferring high entropy air from the low-level eye to the eyewall.

SAR imagery has the advantage of observing features through the clouds at very high spatial resolution, thus the eyewall mesovortices if detected in a SAR image would provide extra evidence that such features do form below the clouds as well. An example of the eyewall mesovortex signature taken on 1 August 2007 at 21:57 UTC by RADARSAT-1 is shown in Fig. 2.1. The vortical structure can be seen at the upper left corner (labeled 'A') of the image which is also located at the inner edge of the eyewall. It is noticed also the filamentary features at the bottom of the eye-eyewall interface in this image (labeled 'B'). Similar features with fingers of high reflectivity extending from the eyewall to the eye have been detected by low-fuselage

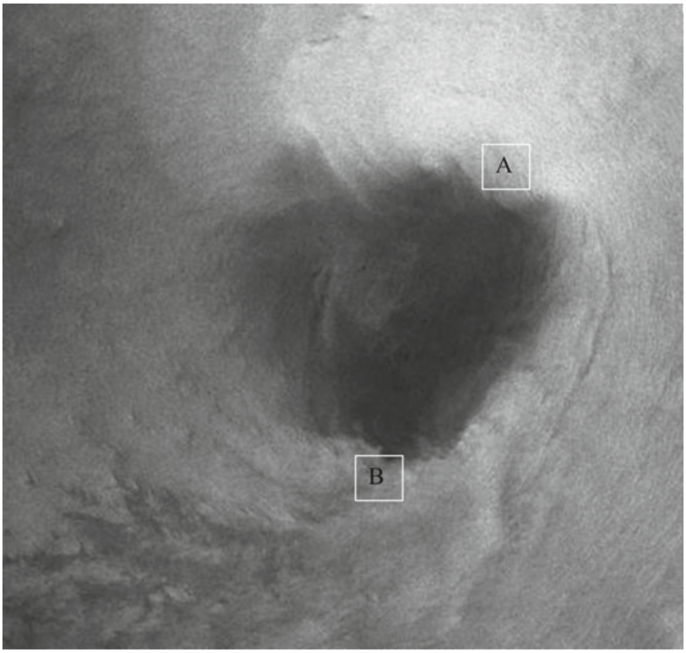

Fig. 2.1 Tropical cyclone eyewall mesovotices observed in a RADARSAT-1 synthetic aperture radar image (copyright Canadian Space Agency) taken in Typhoon Usagi at 20:57:57 UTC on 1 August 2007

radar in Hurricane Isabel on 13 September 2003 as reported by Aberson et al. [28]. They also tracked these features in subsequent radar sweeps and found that they rotate roughly 70–80 m/s. Similar features are also clearly seen in photographs of the eyewall of Hurricane Isabel on 12 September 2003 [28] as well as Hurricane Hugo on 15 September 1989 [25, 29].

Eyewall mesovotices are observed in 3 other SAR images taken in Hurricane Erin on 3 different days (11, 13 and 17 September 2001) (Fig. 2.2a, b, and c). Similar eyewall mesovortex features in Hurricane Erin have been seen in the visible satellite images by Kossin et al. [22]. They suggested a dynamic mechanism to explain the presence of mesovortices in the hurricane eye based on barotropic stability arguments. It is also noticed that the shapes of the eyes in these three images are different, ranging from triangular, square to rectangular. These shapes are associated with the asymmetric dynamics of a hurricane vortex in terms of the azimuthal wavenumbers [30]. Besides the relative strong hurricanes, we also find mesovotices in much weaker cyclones. An example showing mesovortices near the center of Tropical storm Bilis is presented in Fig. 2.3. These mesovortices are believed to be associated with eye-eyewall mixing processes.

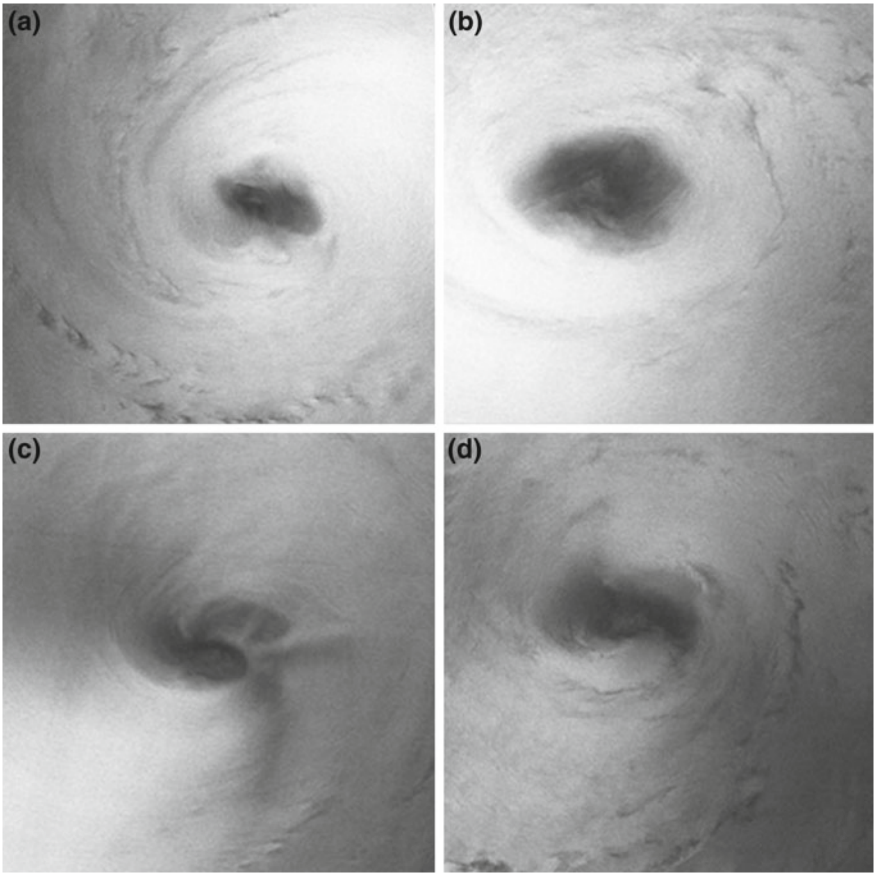

Fig. 2.2 Tropical cyclone eyewall mesovotices observed in RADARSAT-1 synthetic aperture radar images (copyright Canadian Space Agency) taken in **a** Hurricane Erin at 22:19:07 UTC on 11 September 2001; **b** Hurricane Erin at 10:03:10 UTC on 11 September 2001; **c** Hurricane Erin at 8:07:41 UTC on 11 September 2001; and **d** Hurricane Dean at 23:17:51 UTC on 19 August 2007

2.3 Spiral Rainbands, Fine-Scale Bands and Arc Clouds

Spiral band signatures have been often seen in SAR images taken in tropical cyclones. Figure 2.4 show examples of different types of spiral bands not only in their shapes but also in their degree of brightness. Li et al. [30] pointed out that the bright and dark patterns of the spiral bands are associated different physical mechanisms that change the sea surface roughness. These mechanisms are attenuation due to heavy rain; backscattering from rain drops in the air and ice particles; sea surface capillary waves induced by rain; damping of sea surface waves by rain-induced turbulence; and wind gusts [31, 32]. These spiral bands produce large amounts of rainfall and often lead to very costly and potential flooding for landfalling storms.

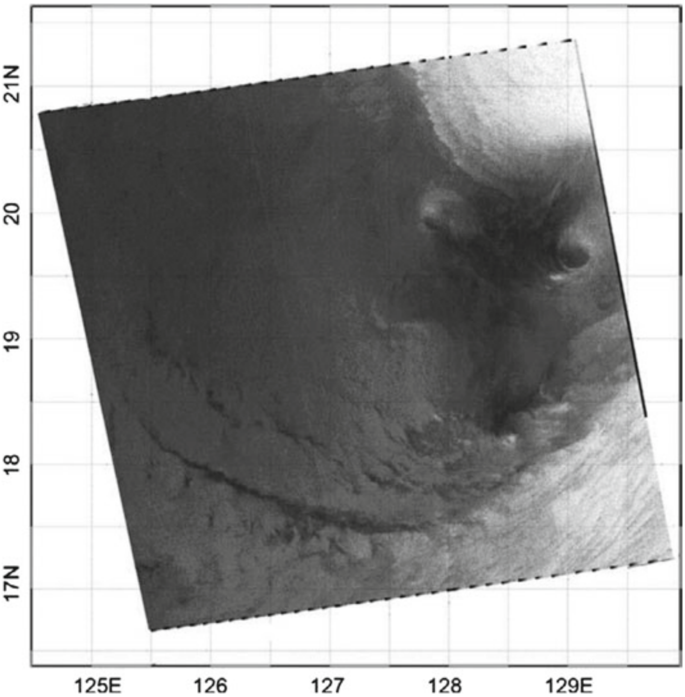

Fig. 2.3 Hurricane eyewall mesovotices observed in a RADARSAT-1 synthetic aperture radar image (copyright Canadian Space Agency) taken in Tropical storm Bilis at 09:35:42 UTC on 11 July 2006

Most tropical cyclones exhibit a set of spiral bands, so called rainbands [33, 34]. The rainbands exhibit a variety of internal structures with deep convective cores embedded in stratiform precipitation [35–37]. The pattern of rainbands in a tropical cyclone is always evolving with different shapes and wavelengths as indicated by Fig. 2.4. Some of the rainbands (Fig. 2.4d) are large with connection to the eyewall. Previous studies suggest that in some intense storms, principal and/or secondary rainbands may evolve into a secondary eyewall triggering eyewall replacement cycle and influencing the storm intensity [37]. Many previous observational studies [35, 36, 38, 39] found decreasing hurricane inflow and decreasing equivalent potential temperature in conjunction with the hurricane rainbands, which are related to the amount of convective activity and thus may have a direct impact of the overall intensity of the parent hurricane.

Arc clouds have been reported to consistently form in the periphery of tropical cyclones as noticed in visible satellite images [40]. Like a primary rainbands, an arc cloud can have a length on the order of several hundred kilometers. Evidence of arc cloud features can be seen in SAR images. For instance, Fig. 2.4b shows a well-organized arc cloud (labeled by "B") in Hurricane Maria on 5 September 2005 at 21:37:58 UTC. It is thought that the presence of arc clouds in the SAR images

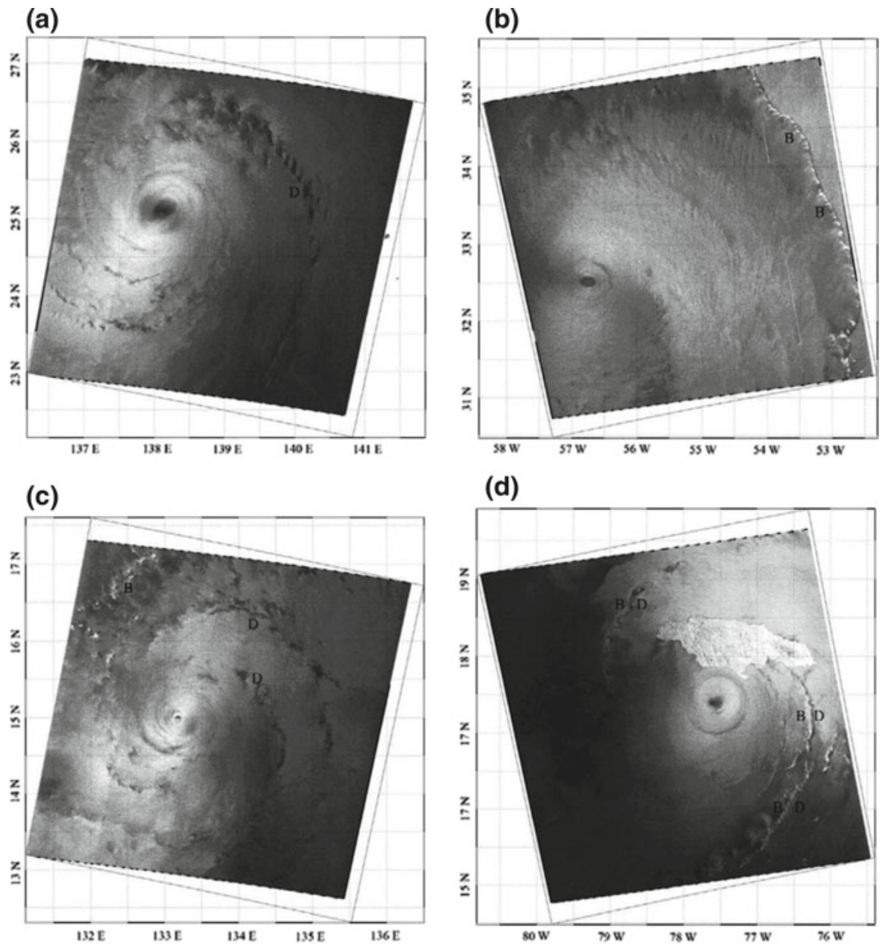

Fig. 2.4 Tropical cyclone spiral band patterns observed in SAR images (All RADARSAT-1 images copyright Canadian Space Agency). Panel **a** shows *dark* rain band pattern in Typhoon Guchol at 20:38:49 UTC on 22 August 2005; Panel **b** shows *bright* rain band pattern in Hurricane Maria at 21:37:58 UTC on 5 September 2005; Panel **c** shows *dark* pattern in inner rain band and *bright* pattern in outer rain band in Typhoon Ewiniar at 20:53:52 UTC on 3 July 2006; Panel **d** shows *bright-dark* pattern in the same rain band in Hurricane Dean at 23:16:40 UTC on 9 August 19 2007. Panel **b** also clearly reveals the signature of arc clouds. Letters "*B*" and "*D*" stand for "*Bright*" and "*Dark*", respectively. The figure is adapted from Li et al. [30]

is due to rain effects. Since we can estimate the surface wind speed from the SAR images, how the arc clouds affect surface winds can be quantified in future work. It is hypothesized by Dunion et al. [40] that arc clouds created low-level outflow may counter the typical low-level inflow that is vital for tropical cyclone formation and maintenance.

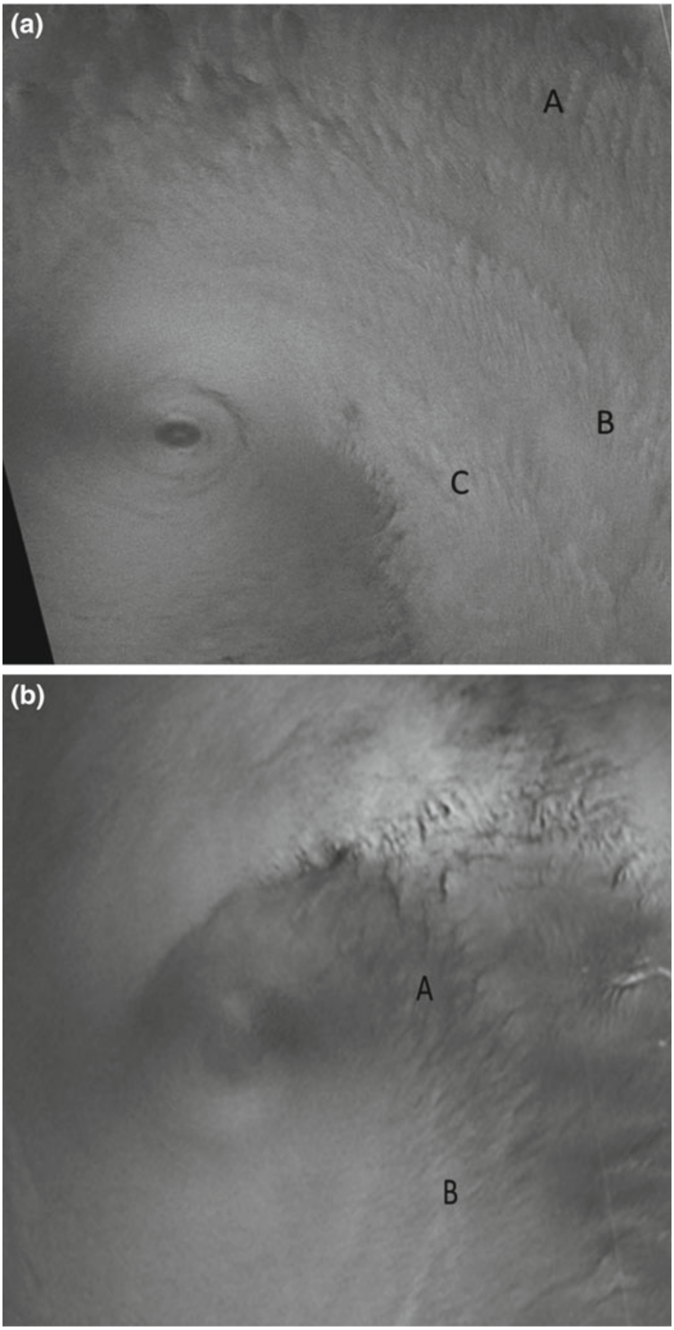

Fig. 2.5 Tropical cyclone fine-scale bands observed in RADARSAT-1 synthetic aperture radar images (copyright Canadian Space Agency) taken in **a** Hurricane Maria at 21:37:58 UTC on 5 September 2005; and **b** Hurricane Maria at 21:21:42 UTC on 9 September 2005. Letters "*A*", "*B*", and "*C*" indicate locations of fine scale bands

As mentioned earlier, another type of spiral bands, "fine-scale spiral bands", with wavelengths of 5–10 km have been identified using Doppler radar data [9]. Using SAR images, Katsaros et al. [13] identified roll-like structures with similar and slightly smaller wavelengths. We also detected fine-scale band signatures in several SAR images in hurricanes. An example is shown in Fig. 2.5 with two SAR images taken in Hurricane Maria on 5 and 9 September 2005, respectively. Features with scales larger than boundary layer rolls but much smaller than a typical primary rainband can be seen (labeled by "*A*", "*B*", "*C*") in these two images. These fine-scale spiral bands are believed to be related to the boundary layer inflection instability [14].

2.4 Boundary Layer Rolls

Boundary layer (BL) rolls or 'roll vortices' can have a significant influence on turbulent exchange of momentum, sensible heat and latent heat in the tropical cyclone boundary layer which are essential for its maintenance and intensification [21]. Foster [19] has developed a theory for roll vortices in curved flow at high wind

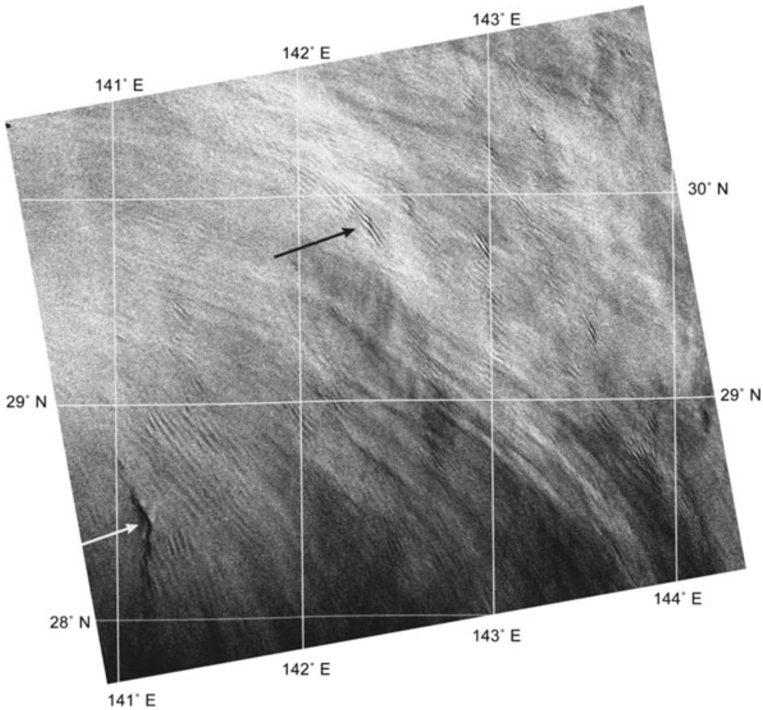

Fig. 2.6 Tropical cyclone boundary layer rolls observed in a RADARSAT-1 synthetic aperture radar image (copyright Canadian Space Agency) taken in Typhoon Fengshen at 08:32:28 UTC on 24 Jul 2002. The figure is adapted from Morrison et al. [16]

speeds, such as in hurricanes, suggesting that tropical cyclone boundary layer is a favorable environment for roll formation.

SAR can provide useful information for identifying tropical cyclone boundary layer rolls, because streak patterns in sea surface roughness can be explained by change in surface wind speed due to the formation of the rolls. Previous studies [13, 16, 19] have presented SAR images clearly showing the roll signatures. Figure 2.6 shows an example of roll signatures in a SAR image taken in Typhoon Fengshen (2002).

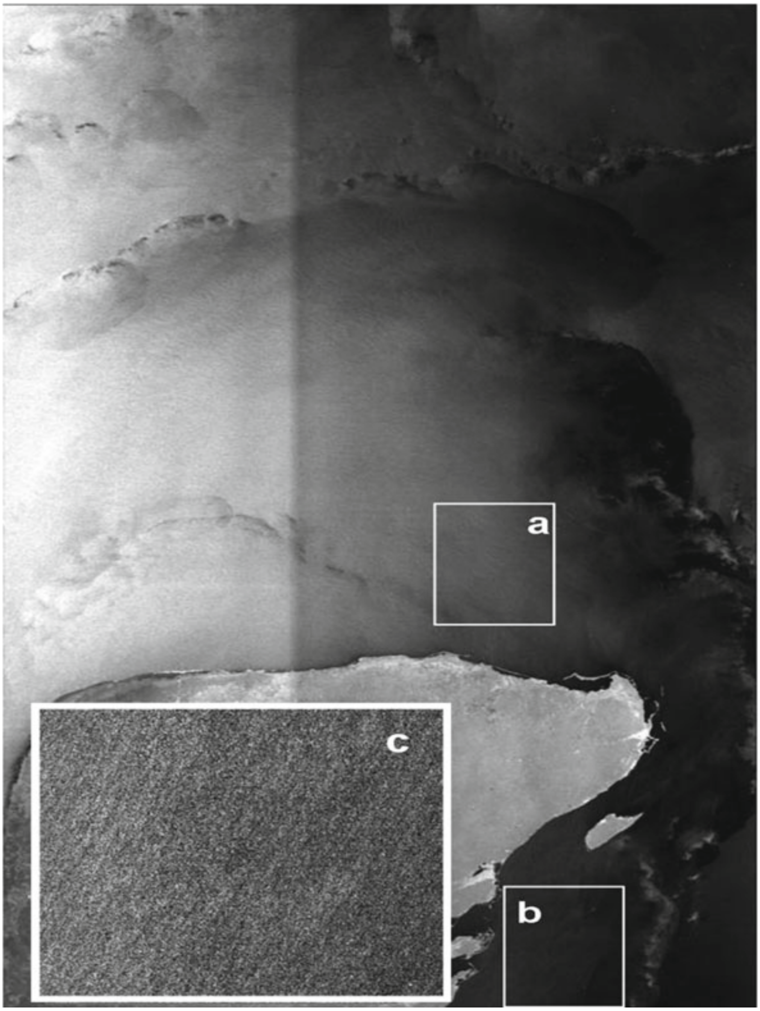

Fig. 2.7 Tropical cyclone boundary layer rolls observed in a RADARSAT-1 synthetic aperture radar image (copyright Canadian Space Agency) taken in Hurricane Isidore at 23:57 UTC on 23 September 2002 after landfall on the Yucatan Peninsula. Analyses of this image and the two boxes are shown in Fig. 2.8. The figure is adapted from Zhang et al. [21]

A RADARSAT-1 SAR image over Hurricane Isidore taken at 23:57 UTC on 23 September 2002 was analyzed by Zhang et al. [21]. At that time, the storm center was nearly stationary over the Yucatan. The SAR image, shown in Fig. 2.7, was first split into subscenes of 20 km (256 pixels of 50 m length and width). A two dimensional Fast Fourier Transform (2D-FFT) algorithm was then used to calculate the directional image spectra for each subscene [41]. The maximum of the 2D spectrum is due to wind streaks or rolls. The direction of the rolls is then taken to be the wind direction.

The analysis result of this SAR image in terms of the wavelength of the rolls is shown in Fig. 2.8. The upper left panel shows the wavelength and direction of the wind streaks. The histogram of the wavelengths of the rolls for the entire image is shown in the upper right panel of Fig. 2.8, indicating a maximum in the distribution of ∼850 m. The lower two panels in Fig. 2.8 demonstrate the analyses of the two boxes of interest as indicated in Fig. 2.7. The wavelengths of the rolls in these two boxes vary from around 400–1100 m, suggesting how the scales of rolls may vary

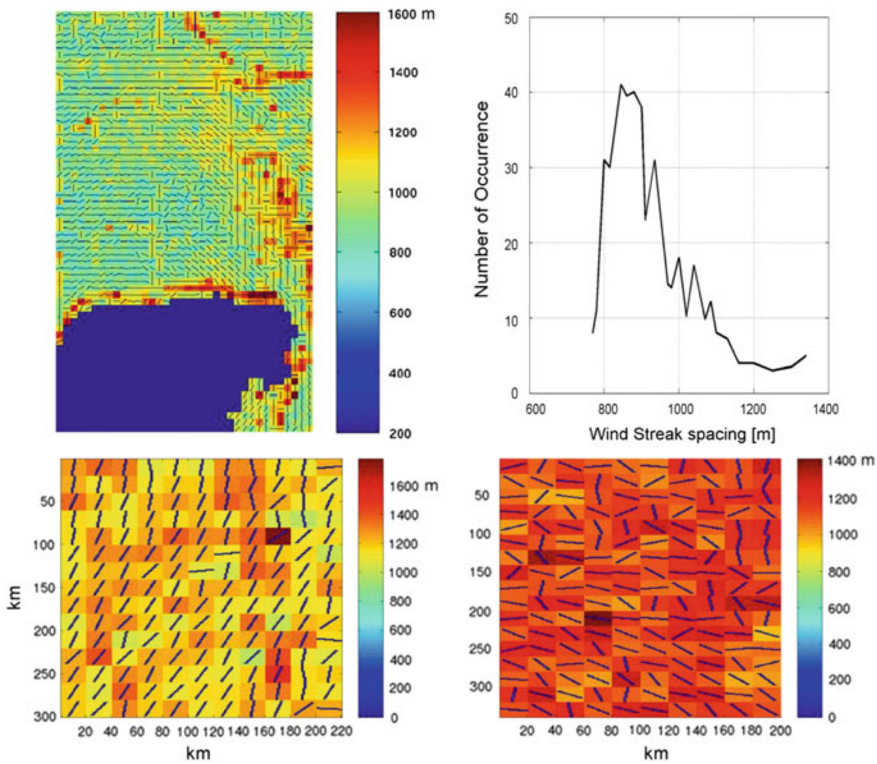

Fig. 2.8 Analysis result of the SAR image in Fig. 2.7. The *upper left panel* shows the wavelength (*color bar code*, m) and direction of the wind rolls. The *upper right panel* shows the histogram of the roll wavelengths of the entire image at *left*. The lower two (*left/right*) *panels* show the wavelength and direction analysis of the (*lower/upper*) *boxes* in Fig. 2.7. The figure is adapted from Zhang et al. [21]

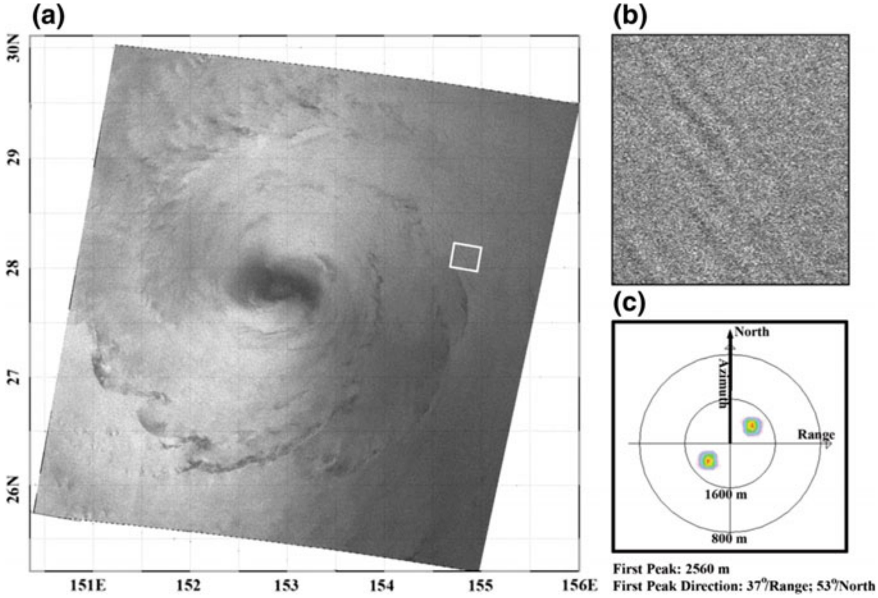

Fig. 2.9 Analysis of boundary layer rolls within Typhoon Fitow. Panel **a** shows a SAR image acquired at 19:42:51 UTC on 1 August, 2007. Full resolution subimage in the *white box* is shown in **b** and its two dimensional FFT analysis in **c**, shows the dominant wavelength and orientation of the boundary layer rolls with 180° ambiguity. The dominant wavelength is 2560 m and its direction is 37° (53°) with respect to the satellite flying range (true North) direction. The figure is adapted from Li et al. [30]

within a storm. The average wavelength of the rolls from the SAR image analysis is generally consistent with that estimated using in-situ aircraft flight-level data.

Another example of boundary layer roll analysis is demonstrated in Fig. 2.9 for a SAR image taken in Typhoon Fitow at 1942 UTC on 1 August 2007. FFT analysis (Fig. 2.9c) on a full-resolution subimage (Fig. 2.9b) shows the spatial dimension of 2–3 km for the wind streaks. The boundary layer rolls are also found to be generally in line with the wind direction. These characteristics of rolls are in agreement with those found from previous studies using Doppler radar data [16, 18].

We note that most previous observational studies on rolls in the tropical cyclone boundary layer to date have mainly focused on landfalling storms. At this point it remains unclear how frequently boundary layer rolls occur in hurricanes, especially in open-ocean conditions. How tropical cyclone boundary layer rolls modulate the mean and turbulence structure remains poorly understood either. With the extensive SAR images taken in tropical cyclones, quantifying the characteristics and mechanisms of tropical cyclone boundary layer rolls becomes promising [30].

2.5 Summary

It is a relatively new tool for tropical cyclone research and forecasting to use a SAR imagery to study its structure and dynamics. This study demonstrates the advantage of SAR sensors for imaging multiscale wind features on the sea surface beneath the storm clouds. Examples of eyewall mesovotices, spiral rainbands, fine-scale bands, arc clouds, and boundary layer rolls are clearly presented. Since SAR images view the actual ocean surface responses to the storm-forced winds with high spatial resolution (<100 m), they provide evidence for the interaction between the multiscale wind features and the surface. These wind features may enhance damages when observed during tropical cyclone landfalls. Qualitative analyses of the characteristics of boundary layer rolls show consistency with previous observations using Doppler radar and/or aircraft flight-level data. This result suggests that a SAR image has potential to be used to improve our understanding of such wind features.

Since the number of spaceborne SAR satellites will increase in the coming years, more collocated observations of tropical cyclones from different spaceborne, airborne and in situ sensors will be obtained. These observations will provide guidance for mapping tropical cyclone surface wind vector in high resolution [42]. They will also help improve our understanding of the mechanisms of the formation of the multiscale wind features. How the tropical cyclone intensity is linked to these wind features can also be investigated with collocated SAR images and other in-situ observations in the future.

References

1. Pielke Jr., R.A., and C.W. Landsea. 1998. Normalized hurricane damages in the United States: 1925–1995. *Weather and Forecasting* 13 (3): 621–631.
2. Marks Jr., F.D., and R.A. Houze Jr. 1984. Airborne doppler radar observations in Hurricane Debby. *Bulletin of the American Meteorological Society* 65 (6): 569–582.
3. Kossin, J.P., and W.H. Schubert. 2004. Mesovortices in Hurricane Isabel. *Bulletin of the American Meteorological Society* 85 (2): 151–153.
4. Reasor, P.D., M.D. Eastin, and J.F. Gamache. 2009. Rapidly intensifying Hurricane Guillermo (1997). Part I: Low-wavenumber structure and evolution. *Monthly Weather Review* 137 (2): 603–631.
5. Braun, S.A., M.T. Montgomery, and Z. Pu. 2006. High-resolution simulation of Hurricane Bonnie (1998). Part I: The organization of eyewall vertical motion. *Journal of the Atmospheric Sciences* 63 (1): 19–42.
6. Nolan, D.S., J.A. Zhang, and D.P. Stern. 2009. Evaluation of planetary boundary layer parameterizations in tropical cyclones by comparison of in situ observations and high-resolution simulations of Hurricane Isabel (2003). Part I: Initialization, maximum winds, and the outer-core boundary layer. *Monthly Weather Review* 137 (11): 3651–3674.
7. Schubert, W.H., M.T. Montgomery, R.K. Taft, T.A. Guinn, S.R. Fulton, J.P. Kossin, and J.P. Edwards. 1999. Polygonal eyewalls, asymmetric eye contraction, and potential vorticity mixing in hurricanes. *Journal of the Atmospheric Sciences* 56 (9): 1197–1223.
8. Kossin, J.P., and W.H. Schubert. 2001. Mesovortices, polygonal flow patterns, and rapid pressure falls in hurricane-like vortices. *Journal of the Atmospheric Sciences* 58 (15): 2196–2209.

9. Gall, R., J. Tuttle, and P. Hildebrand. 1998. Small-scale spiral bands observed in Hurricanes Andrew, Hugo, and Erin. *Monthly Weather Review* 126 (7): 1749–1766.
10. Chen, Y., and M. Yau. 2001. Spiral bands in a simulated hurricane. Part I: Vortex Rossby wave verification. *Journal of the Atmospheric Sciences* 58 (15): 2128–2145.
11. Wang, Y. 2002a. Vortex Rossby waves in a numerically simulated tropical cyclone. Part I: Overall structure, potential vorticity, and kinetic energy budgets. *Journal of the Atmospheric Sciences* 59 (7): 1213–1238.
12. Wang, Y. 2002b. Vortex Rossby waves in a numerically simulated tropical cyclone. Part II: The role in tropical cyclone structure and intensity changes. *Journal of the Atmospheric Sciences* 59 (7): 1239–1262.
13. Katsaros, K.B., P.W. Vachon, W.T. Liu, and P.G. Black. 2002. Microwave remote sensing of tropical cyclones from space. *Journal of Oceanography* 58 (1): 137–151.
14. Nolan, D.S. 2005. Instabilities in hurricane-like boundary layers. *Dynamics of Atmospheres and Oceans* 40 (3): 209–236.
15. Wurman, J., and J. Winslow. 1998. Intense sub-kilometer-scale boundary layer rolls observed in Hurricane Fran. *Science* 280 (5363): 555–557.
16. Morrison, I., S. Businger, F. Marks, P. Dodge, and J.A. Businger. 2005. An observational case for the prevalence of roll vortices in the hurricane boundary layer. *Journal of the Atmospheric Sciences* 62 (8): 2662–2673.
17. Lorsolo, S., J.L. Schroeder, P. Dodge, and F. Marks Jr. 2008. An observational study of hurricane boundary layer small-scale coherent structures. *Monthly Weather Review* 136 (8): 2871–2893.
18. R. Ellis, and S. Businger. Helical circulations in the typhoon boundary layer. *Journal of Geophysical Research: Atmospheres*, 115(D6), 2010.
19. Foster, R.C. 2005. Why rolls are prevalent in the hurricane boundary layer. *Journal of the Atmospheric Sciences* 62 (8): 2647–2661.
20. Fu, L.L., and B. Holt. 1982. Seasat views oceans and sea ice with synthetic aperture radar. *JPL Publication* 81: 120.
21. Zhang, J.A., K.B. Katsaros, P.G. Black, S. Lehner, J.R. French, and W.M. Drennan. 2008. Effects of roll vortices on turbulent fluxes in the hurricane boundary layer. *Boundary-Layer Meteorology* 128 (2): 173–189.
22. Kossin, J.P., B.D. McNoldy, and W.H. Schubert. 2002. Vortical swirls in hurricane eye clouds. *Monthly Weather Review* 130 (12): 3144–3149.
23. Montgomery, M.T., V.A. Vladimirov, and P.V. Denissenko. 2002. An experimental study on hurricane mesovortices. *Journal of Fluid Mechanics* 471: 1–32.
24. Wakimoto, R.M., and P.G. Black. 1994. Damage survey of Hurricane Andrew and its relationship to the eyewall. *Bulletin of the American Meteorological Society* 75 (2): 189–200.
25. Marks, F.D., P.G. Black, M.T. Montgomery, and R.W. Burpee. 2008. Structure of the eye and eyewall of Hurricane Hugo (1989). *Monthly Weather Review* 136 (4): 1237–1259.
26. Montgomery, M.T., M.M. Bell, M.L. Black, and S.D. Aberson. 2006. *Hurricane Isabel (2003): New insights into the physics of intense storms, Part I: Mean vortex structure and maximum intensity estimates*.
27. Emanuel, K.A. 1986. An air-sea interaction theory for tropical cyclones. Part I: Steady-state maintenance. *Journal of the Atmospheric Sciences* 43 (6): 585–605.
28. Aberson, S.D., M.T. Montgomery, M. Bell, and M. Black. 2006. Hurricane Isabel (2003): New insights into the physics of intense storms. Part II. *Bulletin of the American Meteorological Society* 87 (10): 1349.
29. Zhang, J.A., F.D. Marks, M.T. Montgomery, and S. Lorsolo. 2011. An estimation of turbulent characteristics in the low-level region of intense Hurricanes Allen (1980) and Hugo (1989). *Monthly Weather Review* 139 (5): 1447–1462.
30. Li, X., J.A. Zhang, X. Yang, W.G. Pichel, M. DeMaria, D. Long, and Z. Li. 2013. Tropical cyclone morphology from spaceborne synthetic aperture radar. *Bulletin of the American Meteorological Society* 94 (2): 215–230.
31. Bliven, L.F., and J.P. Giovanangeli. 1993. An experimental study of microwave scattering from rain-and wind-roughened seas. *International Journal of Remote Sensing* 14 (5): 855–869.

32. Lin, I.I., W. Alpers, V. Khoo, H. Lim, T.K. Lim, and D. Kasilingam. 2001. An ERS-1 synthetic aperture radar image of a tropical squall line compared with weather radar data. *IEEE Transactions on Geoscience and Remote Sensing* 39 (5): 937–945.
33. Willoughby, H. 1978. A possible mechanism for the formation of hurricane rainbands. *Journal of the Atmospheric Sciences* 35 (5): 838–848.
34. Willoughby. H. 1988. The dynamics of the tropical cyclone core. *Australian Meteorological Magazine* 36 (3).
35. Barnes, G., E.J. Zipser, D. Jorgensen, and F. Marks Jr. 1983. Mesoscale and convective structure of a hurricane rainband. *Journal of the Atmospheric Sciences* 40 (9): 2125–2137.
36. Barnes, G., J. Gamache, M. LeMone, and G. Stossmeister. 1991. A convective cell in a hurricane rainband. *Monthly Weather Review* 119 (3): 776–794.
37. Houze Jr., R.A., S.S. Chen, L. Wen-Chau, R.F. Rogers, et al. 2006. The hurricane rainband and intensity change experiment: Observations and modeling of Hurricanes Katrina, Ophelia, and Rita. *Bulletin of the American Meteorological Society* 87 (11): 1503.
38. Powell, M.D. 1990a. Boundary layer structure and dynamics in outer hurricane rainbands. Part I: Mesoscale rainfall and kinematic structure. *Monthly Weather Review* 118 (4): 891–917.
39. Powell, M.D. 1990b. Boundary layer structure and dynamics in outer hurricane rainbands. Part II: Downdraft modification and mixed layer recovery. *Monthly Weather Review* 118 (4): 918–938.
40. Dunion, J., M. Eastin, D. Nolan, J. Hawkins, and C. Velden. 2010. Arc clouds in the tropical cyclone environment: Implications for TC intensity change. In *Preprints, 29th conference on hurricanes and tropical meteorology, Tucson, AZ, American Meteorological Society C*, Vol. 6.
41. Lehner, S., J. Schulz-Stellenfleth, B. Schattler, H. Breit, and J. Horstmann. 2000. Wind and wave measurements using complex ERS-2 SAR wave mode data. *IEEE Transactions on Geoscience and Remote Sensing* 38 (5): 2246–2257.
42. Zhang, B., W. Perrie, J.A. Zhang, E.W. Uhlhorn, and Y. He. 2014. High-resolution hurricane vector winds from C-band dual-polarization SAR observations. *Journal of Atmospheric and Oceanic Technology* 31 (2): 272–286.

http://www.springer.com/978-981-10-2892-2

Hurricane Monitoring With Spaceborne Synthetic Aperture Radar
Li, X. (Ed.)
2017, XIII, 398 p. 238 illus., 191 illus. in color., Hardcover
ISBN: 978-981-10-2892-2